

HEAT TRANSFER ENHANCEMENT BY TRAVELING WAVE-LIKE BODY FORCE IN TURBULENT CHANNEL FLOW

Ryo Yamamoto, Junichi Morita, Hiroya Mamori, Takeshi Miyazaki

Department of Mechanical and Intelligent Systems Engineering
The University of Electro-Communications
1-5-1 Chofugaoka, Chofu, Tokyo, 182-8585, Japan
mamori@uec.ac.jp

Shmpei Hara

Department of Energy and Mechanical Engineering
Doshisha University
1-3, Tatara Miyakodani, Kyotanabe-shi, Kyoto, Japan

ABSTRACT

Direct numerical simulations of the turbulent channel flow controlled by the traveling wave are performed. We employed the traveling wave-like body force to mimic the self-excited thin film, which has a dissimilar effect on momentum and heat transfer. The dissimilar effect is obtained when the wave travels in the downstream direction of which wavespeed is slower than the bulk velocity. The three-component decomposition shows that the traveling wave generates velocity rotation, which increases the skin-friction drag and heat transfer. In addition, the coherent component of the Reynolds shear stress decreases while that of the turbulent heat flux increases, which is responsible for the dissimilar effect.

INTRODUCTION

Energy consumption is increasing year by year, and population growth and improving energy efficiency is a common issue globally. In fluid engineering, the development of flow control methods to improve energy efficiency has been actively pursued. In particular, research on the reduction of skin-friction drag and enhancement of heat transfer has been frequently conducted. It is known that there is a similarity between heat and momentum transport. Especially in turbulent flows, vortical structures promote the heat and momentum transports, and heat transfer and skin-friction drag are increased. However, increasing the heat transport and reducing (or increasing slightly) the skin-friction drag simultaneously are required, and dissimilar controls have been investigated.

Hasegawa & Kasagi (2011) derived a control law based on the sub-optimal theory using the intrinsic difference between velocity and temperature. The law was applied to the control of blowing and suction from walls. Direct numerical simulations (referred to as DNS) in the turbulent channel flow with the control were performed. They obtained tripled heat transfer with doubled skin-friction drag as compared with the uncontrolled case. Yamamoto *et al.* (2013) performed the DNS of the turbulent channel flow controlled by the wall transpiration based on the optimal control theory. They obtained a 30 % reduction of the skin-friction drag and doubled the heat trans-

fer. Kaithakkal *et al.* (2020) confirmed the dissimilar effect by a traveling wave-like blowing and suction in the turbulent channel flow. Instead of the blowing and suction from the wall, Murakami & Hara (2020) made an experimental study of the channel flow to investigate the dissimilar effect of the traveling wave. They employed a self-excited thin film installed apart from the walls and confirmed the dissimilarity, which depended on the distance between the film and the wall.

In this study, we reproduce the experiment of Murakami & Hara (2020) by direct numerical simulations. Instead of the self-excited thin film, we employed the traveling wave-like body force control. The purpose is to investigate the effect of the control on the dissimilar control effect and clarify the mechanism.

DIRECT NUMERICAL SIMULATION

The DNS of the turbulent channel flow with the traveling wave-like body force control is performed. The governing equations are the continuity, the Navier-Stokes, and the energy equations of the incompressible flow, as

$$\frac{\partial u_i}{\partial x_i} = 0, \quad (1)$$

$$\frac{\partial u_i}{\partial t} + \frac{\partial u_i u_j}{\partial x_j} = -\frac{\partial P}{\partial x_i} + \frac{1}{\text{Re}_\tau} \frac{\partial^2 u_i}{\partial x_j \partial x_j} + f_i, \quad (2)$$

$$\frac{\partial T}{\partial t} + \frac{\partial u_j T}{\partial x_j} = Q + \frac{1}{\text{Re}_\tau \cdot \text{Pr}} \frac{\partial^2 T}{\partial x_j \partial x_j}, \quad (3)$$

Here, t is time, P is pressure, T is temperature, Q is heat source and f_i is the body force term. The streamwise, wall-normal, and spanwise directions are defined as x , y , and z , respectively, and the corresponding velocity components are defined as u , v , and w . We interchangeably use x_i and u_i ($n = 1 \sim 3$) as the coordinate and the velocity in this paper. The mean pressure gradient in the streamwise direction is kept constant, and the friction Reynolds number is set to 180. The Reynolds number is defined by the reference values of the channel half-width δ^*

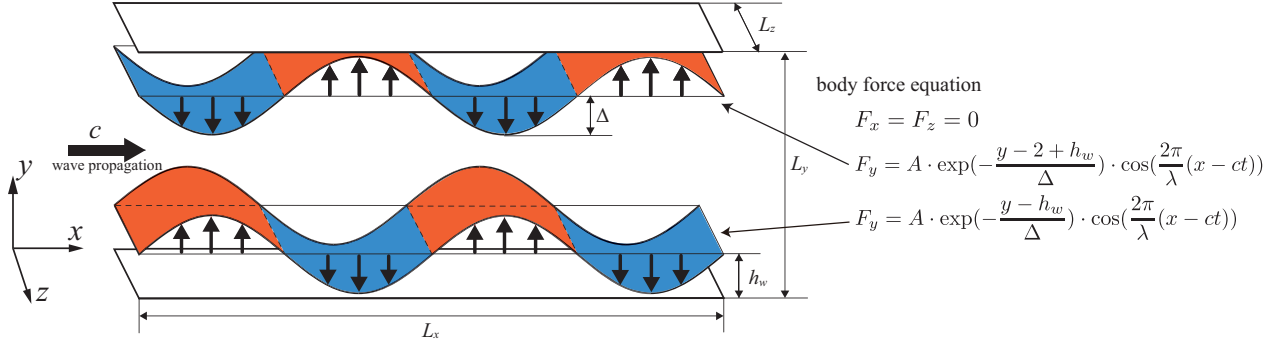


Figure 1. Schematics of the channel flow with the traveling wave-like body force.

and the wall-friction velocity u_τ^* . To hold an analogy between the momentum and heat transfer, we imposed a uniform heat generation condition and a Prandtl number of $Pr = 1$. The governing equations are discretized by using an energy-conserving second-order central difference method. As time advances, we employ the second-order Crank-Nicolson method for the viscous term and the low storage third-order Runge-Kutta method for the other terms.

Figure 1 shows the schematic of the channel flow with the traveling wave control. The computational domain is $(L_x, L_y, L_z) = (2\pi, 2, \pi)$ and the grid points are $(N_x, N_y, N_z) = (256, 384, 128)$. The periodic boundary conditions are imposed in the streamwise and spanwise directions, and the no-slip condition is imposed on the wall. The temperature on the wall is zero. We note that the body force control allows for flowing penetration of the flow through the film, unlike the corresponding experiment by Murakami & Hara (2020). As shown in Fig. 1, the control parameters are the amplitude A , the penetration length Δ , the control position h_w , wavelength λ , and the wavespeed c . The paper shows the effect of wavespeed c while the others are fixed at $A = 500$, $\Delta = 0.1$, $h_w = 0.5$, and $\lambda = \pi$.

RESULT AND DISCUSSION

Figure 2 shows the control effect of the wavespeed c as a function of a skin-friction drag coefficient C_f , a Nusselt number Nu , as

$$C_f = \frac{\tau_w^*}{\frac{1}{2}\rho^*U_b^*}, \quad (4)$$

$$Nu = \frac{2\delta^*h^*}{\lambda^*}, \quad (5)$$

Here, τ_w^* is the wall shear stress, ρ^* is the fluid density, U_b^* is the bulk velocity, h^* is the heat transfer coefficient, and λ^* is the thermal conductivity. The asterisk means the dimensional variables. In addition, the dissimilarity is evaluated by j/f factor, as

$$j/f = \frac{Nu}{Pr^{1/3}Re_b} \frac{1}{4C_f}, \quad (6)$$

where Re_b is the bulk Reynolds number. These are normalized by the uncontrolled values. Figure 2(a) shows the dependency of c , and the other parameters are fixed at $h_w = 0.5$, $\Delta = 0.1$, $A = 500$, and $k = 2$. We found that the downstream traveling

wave at $0 < c < 30$ affects the cost functions. The skin-friction coefficient and the Nusselt number peak at $c = 10$. Because the j/f is positive and maximum, the increment of the heat transfer is larger than that of the skin-friction drag. It implies the dissimilarity effect and we chose $c = 10$ as a reference case in the following. Figure 2(b) shows the dependency of h_w on $\Delta = 0.1$, $A = 500$, $c = 11$, and $k = 2$. The Nusselt number and skin-friction coefficient increase with an increase in h_w , whereas they slightly decrease at large values of h_w . Moreover, the j/f factor increases, and the maximum value is obtained at $h_w = 0.6$.

Figure 3 compares the instantaneous streamwise velocity between the uncontrolled flow and the reference case. The white isosurface shows the vortical structure visualized by the second invariant of the velocity deformation tensor (so-called the Q value), while the thresholds are 0.03 for the uncontrolled flow and 0.17 for the reference case. As a result, the turbulence is well promoted by the traveling wave in the reference case. In the uncontrolled case, the vortical structures are in the region near the wall. On the other hand, the vortical structures clustered and distributed alternately in the streamwise direction in the reference case.

We introduce a three-component decomposition method to investigate the contribution of the traveling wave to the flow. Previous studies have distinguished contributions based on the direct and indirect effects of traveling waves Mamori & Fukagata (2014). Accordingly, we define the three-component decomposition method for an arbitrary quantity f as

$$f = \bar{f} + f' \\ = \langle f \rangle + f'' = \bar{f} + \tilde{f} + f'', \quad (7)$$

where \bar{f} and $\langle f \rangle$ are defined as

$$\bar{f}(y) = \frac{1}{2\pi} \int_0^{2\pi} \langle f \rangle d\phi_x, \quad (8)$$

$$\langle f \rangle(\phi_x, y) = \frac{1}{N_{\phi_x}} \sum_{x \in \phi_x} \left[\frac{1}{\mathcal{T}L_z} \int_0^{\mathcal{T}} \int_0^{L_z} f(x, y, z, t) dz dt \right], \quad (9)$$

where $\phi_x = k(x - ct) - 2\pi n$ ($0 < \phi_x < 2\pi, n \in \mathbb{Z}$) is the wave coordinate along the streamwise direction and $N_{\phi_x} = kL_x / (2\pi)$ is the number of streamwise locations belonging to the same phase. The RSS ($-\overline{u'v'}$) and THF ($-\overline{v'T'}$) are decomposed using the three-component decomposition method as

$$-\overline{u'v'} = -\overline{\tilde{u}\tilde{v}} - \overline{u''v''}, \quad (10)$$

$$-\overline{v'T'} = -\overline{\tilde{v}\tilde{T}} - \overline{v''T''}. \quad (11)$$

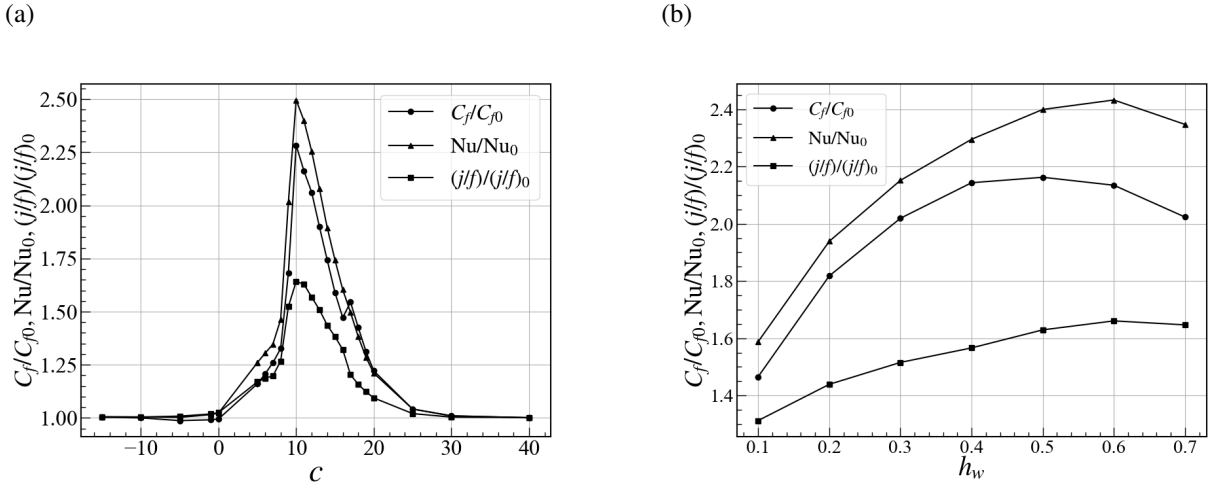


Figure 2. Dependency of (a) c ($h_w = 0.5$, $\Delta = 0.1$, $A = 500$, and $k = 2$) and (b) h_w ($\Delta = 0.1$, $A = 500$, $c = 11$, and $k = 2$) on the skin-friction coefficient, Stanton number, and j/f factor. They are normalized to those of the uncontrolled values.

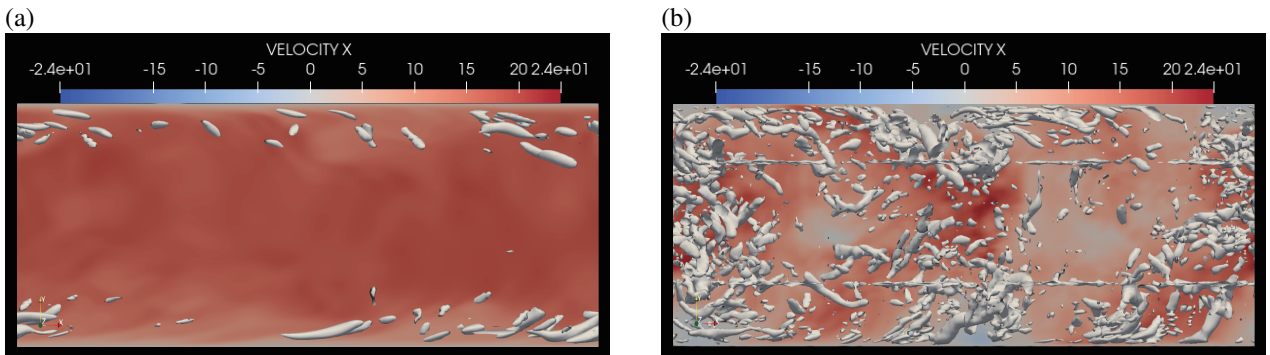


Figure 3. Instantaneous streamwise velocity in (a) the uncontrolled case and (b) the reference case on the $x-y$ plane between $z = 0$ to $z = \pi/2$. The threshold values of the vortical structures are $Q^+ = 0.03$ and $Q^+ = 0.17$ for uncontrolled case and reference case, respectively.

The LHS is referred to as the “total” component, and the first and second terms on the RHS are referred to as the “coherent” and “random” components.

The RSS and THF significantly influenced on the skin-friction coefficient and Nusselt number. The decomposed RSS and THF in each case are shown in Fig. 4. For the controlled cases (Cases 1~3), other control parameters are fixed at $\Delta = 0.1$, $A = 500$, $c = 11$, and $k = 2$. The total-RSS in Case 1 is slightly larger than that of Case NC; the random-RSS almost agrees with the total-RSS, and the coherent-RSS is very small. When h_w increases, the coherent-RSS decreases, and the random-RSS increases in Case 2; the peaks slightly decrease and shift toward the channel center in Case 3. The total-THF and coherent-THF are positive. The coherent-THF peaks in the region near the wall in Case 1, whereas it attenuates and moves toward the channel center as h_w increases in Cases 2 and 3. However, the random-THF had double peaks in Case 1, but the near-wall peak grows, and the other peak decreases and disappears in Cases 2 and 3.

CONCLUSION

The direct numerical simulations of the turbulent channel flow controlled by traveling waves are performed. We employ the traveling wave-like body force to mimic the self-excited thin film and investigate the effects on skin-friction drag and heat transfer. The downstream traveling wave obtains the dissimilar effect between momentum and heat transfers, and it

peaks at $c = 10$. In addition, depending on the control position, the j/f factor increases, and the maximum value is obtained at $h_w = 0.6$. The three-component decomposition indicates that the traveling wave generates rotation of the velocity. The contribution of the coherent component is different between the RSS and THF: the coherent-RSS decreases, and the coherent-THF increases. It is responsible for the dissimilarity between momentum and heat transfers.

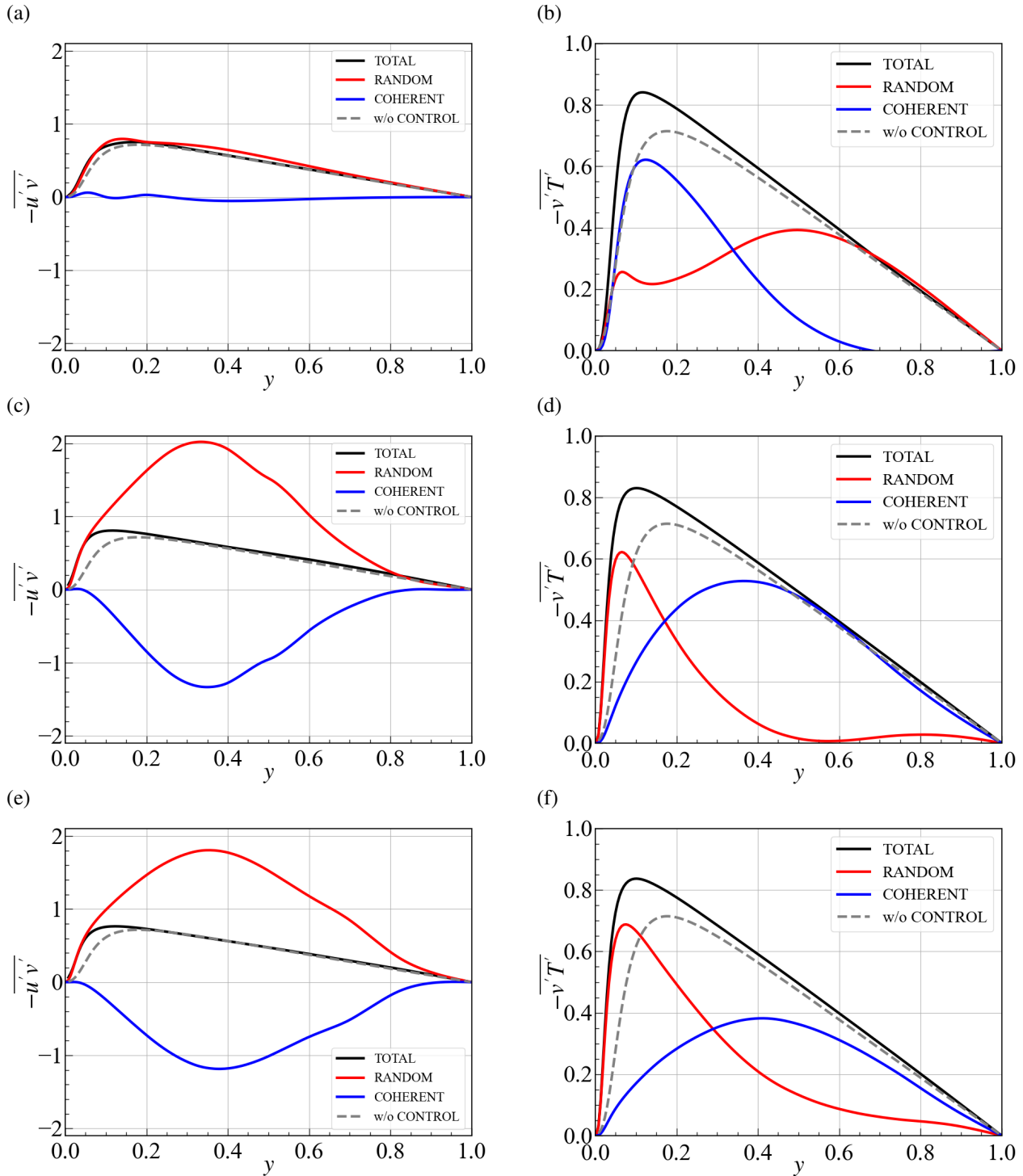


Figure 4. Decomposed Reynolds share stress (left) and turbulent heat flux (right): top, Case 1; center, Case 2; bottom, Case 3. Black, total-RSS; red, random-RSS; blue, coherent-RSS; broken line, Case NC.

REFERENCES

- Hasegawa, Y. & Kasagi, N. 2011 Dissimilar control of momentum and heat transfer in a fully developed turbulent channel flow. *Journal of Fluid Mechanics* **683**, 57–93.
- Kaithakkal, A. J., Kametani, Y. & Hasegawa, Y. 2020 Dissimilarity between turbulent heat and momentum transfer induced by a streamwise travelling wave of wall blowing and suction. *Journal of Fluid Mechanics* **886**, 1045.
- Mamori, H. & Fukagata, K. 2014 Drag reduction effect by a wave-like wall-normal body force in a turbulent channel

flow. *Physics of Fluids* **26** (115104).

- Murakami, T. & Hara, S. 2020 Influence of the installation of a rubber sheet on pressure drop and heat transfer characteristics in turbulent channel flow. *In Proc. 57th annual meeting of the heat transfer society of Japan* (B211).
- Yamamoto, A., Hasegawa, Y. & Kasagi, N. 2013 Optimal control of dissimilar heat and momentum transfer in a fully developed turbulent channel flow. *Journal of Fluid Mechanics* **733**, 189–220.